Silk-Magnesium Composite Based Orthopedic Wire for Toe Fusion Surgery: Balancing Biodegradability and Preserving Native Toe Orientation

A thesis submitted by
Emily Frances Day
In partial fulfillment of the requirements for the degree of
Master of Science in Biomedical Engineering
Tufts University
August 2024

Advisor: David Kaplan, PhD

Thesis committee:

David Kaplan, PhD
Chunmei Li, PhD
Samuel L Lin, MD

Abstract

Arthrodesis or surgical fixation of the bones in the toes using a stainless-steel k wire is a common surgery used to fix toe deformities such as hallux valgus and hammer toe. However, repeated hospital visits and uncomfortable healing conditions have prompted the need for an alternative. To target these restrictions in the current K-wire design, a biodegradable alternative has been developed which incorporates the anatomical orientation of the toe joint as it heals, allowing for a more comfortable patient experience. As such, a silk fibroin (SF) thermoplastic reinforced with a 99.9% magnesium (Mg) wire creates a strong and thermoformable composite capable of holding the ends of the joint in place and molding to the native toe orientation shape, allowing for fusion and a more comfortable patient experience and subsequent outcome. The application of hydrophobic coatings on the surface of the magnesium wire is intended to block water infiltration and reduce the risk of premature degradation.

This study aims to mechanically assess the performance of these biodegradable composites in both hydrated and dry conditions, while also examining their degradation behavior. Fourier Transform Infrared Spectroscopy (FTIR) confirmed the successful polymerization of 16-hydroxyhexadecanoic acid (HHA) to Cutin-inspired poly (hydroxyhexadecanoate) (PHHA). Atomic Force Microscopy (AFM) confirmed coating of the hydrophobic polymers on the surface of the Mg wires. The images indicated a successful coating of Cutin but showed inconsistent coating of poly(lactic-co-glycolic) acid (PLGA).

The moduli collected from three-point bending tests in dry and hydrated condition were consistent with that of brittle and elastic materials, respectively. The composites were capable of withstanding high stress but fell short of native bone and the stainless-steel K wires.

The samples were able to endure 30 days in a protease solution, losing only about half of their mass. This demonstrates their ability to stabilize the joints, facilitating fusion, which typically takes 2-3 months, depending on the patient. Based on the presented data, the SF-Mg composite wires have the potential to be a successful replacement for existing solutions used in toe joint arthrodesis.

Acknowledgements

My experience at Tufts has been both highly rewarding and challenging. Through the breaking of the thermopress for three months to the Instron deciding to not work on the day I was planning on testing all my samples. Things have been a bit chaotic to say the least. But I am still here today, finishing my thesis and presenting the data that I have worked so hard to collect over the past 7 months. For that I thank Dr. Kaplan for not losing faith and always providing supporting. To Reddhy, for her advice and listening when I just needed to talk something out, I truly appreciate your input and help. To Kareen for assuring me that she too made the same mistakes. To Anna, thank you for being the best undergrad out there. If it weren't for you, I would probably still be making samples right now. You are going to go far, and I can't wait to see what the future holds for you. And finally, to arguably my favorite Kaplan lab colleague, Evan. Thank you for your continued support and help. You are the person I talk experiments with, data with, and everything in between. I quite literally would not be here without you, and not just because I used your prism account to make my graphs. I am in awe of your intelligence and dedication, and I can't wait to see what you accomplish. I simply can't thank you enough. To the Kaplan lab as a whole, thank you.

To my friends and family thank you so much for your unrelenting support. To my parents, Soph, Alli and Wyatt, thank you for teaching me to work hard and encouraging me to follow my dreams and never give up. Thank you to my grandparents and Uncles for your unrelenting support. To all my friends, Sammi, Mckenna, Mackenzie, Ali, Codi, Kathryn, Bryce, Sam, Hannah (all three of them), Mina, Lili thank you for constantly lifting my spirits, I am so lucky to have you. To my Maine family thank you for always being my own personal cheerleading team, I couldn't have done it without you. Thank you to my colleagues at Frank's for your continued support and helping to cover shifts when I was stuck in lab, I truly appreciate it. Especially to my UVM mentors, Dr. Doiron, and Dr. Floreani, thank you for your dedication to your job and your enthusiasm, I would not be here without your continued support and encouragement.

In my time in the Kaplan lab, I have become a much better scientist and person, and I am so grateful for my time here. Thank you, Tufts.

Table of Contents

Chapter 1: Introduction

1.1 Toe Deformities

Toe deformities such as hallux valgus and hammer toe are extremely prevalent and cause discomfort and pain during movement, particularly affecting individuals with chronic conditions like arthritis and diabetes[1]. Patients with hallux valgus often develop secondary hammer toe deformities in the lesser toes, particularly when the condition is left untreated[2]. Arthrodesis, commonly known as toe fixation, represents the gold standard in orthopedics for treating these conditions. Specifically, the deformed metatarsophalangeal (MTP) joint and/or proximal interphalangeal (PIP) joint of the toe are affixed utilizing a stiff, straight wire known as a Kirschner wire or K-wire [3].

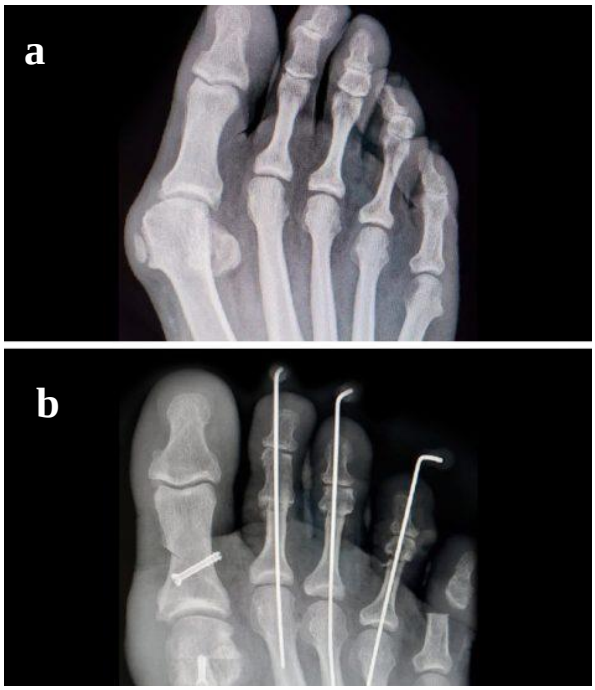

Figure 1. ***Gold Standard Arthrodesis Procedure for K-wire Toe Fixation Surgery*** [4]. ***(a)*** *Deformation of the MTP joints of the big toe and PIP joints of the lesser toes, resulting in a hallux valgus and hammer deformity, respectively.* ***(b)*** *Fixation of the deformed MTP joints using a K-wire. The wire is fixed into the bone throughout the joint and out through the toe. This wire remains in this position for 6 weeks or until proper fusion of the bone occurs*[5].

1.2 The Use of K Wires in Toe Fixation Surgery and their Limitations

K-wires play a pivotal role in arthrodesis, providing essential mechanical stability to fractured or deformed joints. These stiff wires, often composed of materials like 304 stainless

steel, are strategically inserted to immobilize the joint during the healing process, ensuring proper alignment and facilitating bone fusion. The wire extends through the bone and protrudes from the skin. Full toe fusion can typically take about 2-3 months to fuse depending on the patient [5]. Following fusion of the toe, the surgeon removes the wire by extracting the exposed portion allowing for the restoration of joint integrity and function. While this method effectively immobilizes the joint and facilitates bone healing, it also imposes mobility restrictions once healing is complete[6]. The requirement for numerous hospital visits, prolonged presence of protruding K-wires, and limitations in mobility detract from the overall efficacy of this solution[7].

1.3 Recent Technology

Recently, many companies have set out to address these concerns, but their solutions have fallen short of the necessary requirements for a successful product. The Stryker Smart Toe II intramedullary implant aims to apply dynamic compression for hammer toe correction. Although this implant was shown to have less than a 1% rate of implant failure, it still results in the stiffening of the joint and requires removal[8]. Magnezix has recently created a compression screw formulated from a magnesium-based alloy [9]. This device is capable of biodegrading safely within the body, preventing the need for repeated hospital visits, but is still being evaluated for infection and material failure rates [10, 11, 12].

ActivaPin from *bioretec* addresses multiple drawbacks of current technology in this field. More specifically, it also addresses the need for a biodegradable alternative as the device is primarily made of the biodegradable polymer, PLGA. In addition, it is capable of being customized via bending the wire to achieve the desired anatomical orientation [13]. However, PLGA by itself is weaker than other bioresorbable materials such as magnesium, which may result, in failure of the implant[14]. Some defects in postoperative mobility were also reported [15].

The existing solutions mentioned previously exhibit notable technological gaps, emphasizing the necessity for innovative alternatives[16]. In response to these identified gaps, specific aims will be defined to ensure the resultant product effectively addresses these deficiencies in current technology.

1.4 Application of Silk Thermoplastics

Silk consists of fibrous proteins produced by silkworms, specifically the *Bombyx mori.*[17]. The main protein of silk, which is typically extracted for these applications, is silk fibroin (SF).

This protein consists of organized β-sheet crystallites as well as amorphous domains[18]. These structural aspects of silk provide ideal mechanical properties, capability for controlled biodegradability, potential for functionalization, and enhanced biocompatibility[19]. Given the attractive properties of silk, it is already a widely established material in the field of medicine specifically, with applications in surgical sutures. Silk is also widely studied in research for use as scaffolds in tissue engineering of bone and other musculoskeletal tissues[20,21]. More recently, the properties of silk have been exploited to create silk-based thermoplastic materials capable for use as orthopedic screws and potential sustainable building materials[22,23].

Thermoplastics describe a class of polymer materials which become malleable when heated to a specific temperature and harden when cooled. These materials can be reheated, reshaped, and subsequently cooled repeatedly to create a desired shape or orientation. Silk-based thermoplastics are able to retain their notable mechanical strength and biodegradability while also capable of being reheated and remolded according to required specifications[22]. This process is referred to as thermoforming[24].These properties make them attractive for use as a K-wire alternative.

A significant challenge in the use of silk in these applications involves water infiltration. When most silk-based materials are exposed to an aqueous environment, they undergo degradation, leading to a reduction in their favorable mechanical properties and eventual failure of the implant. As such, it is essential to understand the behavior of silk in a hydrated vs. dry state.

1.5 Advantages of Magnesium in Bone Healing

Evidence regarding the contribution of magnesium (Mg) to both osteoinductivity and osteoconductivity has been established[25]. In addition, magnesium can be visualized using medical imaging, allowing for precise placement of the implant. These factors emphasize its ideal utilization in orthopedic technologies.

Considering these factors, the incorporation of a 99.9% pure magnesium wire into a thermoplastic composite aims to assist in the progression of bone fusion in addition to providing additional mechanical strength to the material as a whole. Both components are biocompatible as well as capable of degrading safely within the body [16]. The proposed design is shown in Figure 2.

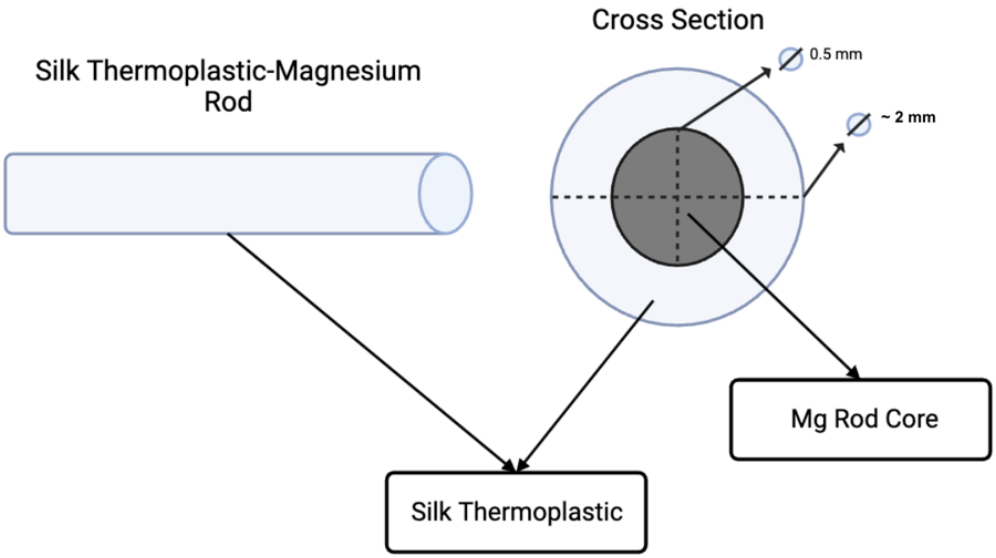

Figure 2. ***Proposed SF-Mg Thermoplastic Composite Schematic.*** *The composite consists of multiple parts, including a 0.5 mm, 99.9% pure Mg wire surrounded by 1% SF. This is then thermopressed together to create a cohesive composite consisting of 1% SF thermoplastic and a Mg wire affixed in the middle.*

1.6 Objective and Aims

The first aim in this study involves the creation of the 1% SF-Mg thermoplastic composites. Novel methods for embedding the magnesium wire into thermoplastics must be created and optimized. This involves creating a system of molds to press Mg the wire directly into the thermoplastic, creating a larger bar with the embedded magnesium wire. This bar must have specifications that are large enough to allow for machining via a lathe to create the desired end wire shape with the specified diameter. To compare these newly formulated wires to the current gold standard and other available technologies, the final composites will need to be machined down to a diameter of 1.5- 2.0 mm. Once this protocol is established, the resultant cohesive thermoplastic containing a straight Mg wire affixed in the middle can be created and further analyzed.

The second aim of this study focuses on preventing premature degradation of the composite in vivo. Given the aqueous environment of the human body, preventing premature degradation of the Mg as a result of corrosion is necessary. As stated before, it has been previously established that when hydrated, silk begins to degrade and lose its desirable mechanical properties. As such, in an aqueous environment, the 1% SF outer portion of the composite would degrade first and leave the magnesium wire to handle the mechanical load,

allowing for the bone to fuse appropriately. As such, a hydrophobic coating must be identified and used to prevent water infiltration and premature degradation of the Mg wire[26]. Various hydrophobic coatings were investigated in an effort to identify the best fit for the given application[27]. Two hydrophobic coatings were chosen, PLGA and PHHA, a Cutin-inspired polymer [28]. The magnesium wires were prepped via surface roughening to allow for greater adhesion between the coating and the wire surface. AFM imaging was used to confirm a homogenous coating and allow for surface visualization of the coating on the Mg wires.

The third aim involves establishing the degradation profile for the composite wires in both protease XIV and PBS solution for 30 days. These studies are to be performed to ensure the composite wires are capable of following the desired degradation timeline to allow for appropriate bone fusion and provide the necessary mechanical support throughout the healing process. The evaluation of these wires aims to provide an advanced understanding of both their performance and stability. The coated samples are anticipated to demonstrate behavior similar to that of the 1% SF samples, as the protease is expected to consistently break down the silk proteins in both types of samples. Overall, the samples placed in the protease XIV solution are expected to degrade faster as compared to those incubated in PBS.

The fourth aim relates to the mechanical evaluation of the composites. The composites must be mechanically evaluated to ensure that they are capable of meeting the mechanical requirements of bone without causing stress shielding or falling below the necessary mechanical strength to support fusion. The mechanical strength values of both native bone and current K-wires were collected for comparison[29]. Three-point bending tests were performed on the composites in both dry and hydrated states as to better understand the behavior of the hydrated silk and its influence on the mechanical behavior given previous challenges. As such, the 1% SF composite wires are expected to be consistent with the behavior in previous literature. The reinforced composites are expected to withstand higher mechanical stress, given the presence of the Mg wires[22]. In addition, the Mg wires are expected to provide mechanical reinforcement. When the SF fails, the Mg takes on the stress and mechanically supports the composite until complete failure.

1.7 Conclusions

This study aims to overcome current restrictions in Arthrodesis or surgical fixation of the bones in the toe. To target these restrictions, a biodegradable alternative was developed which

incorporates the anatomical orientation of the toe joint as it heals, allowing for a more comfortable patient experience. In theory, embedding a 99.9% Mg wire into a silk fibroin thermoplastic creates a strong and thermoformable composite capable of holding the ends of the joint in place to allow for fusion. An illustration of this proposed material is shown in Figure 2. Substituting the 99.9% Mg wire with commercial alloys, as they become available in the future, is anticipated to enhance the strength of these composites, thereby optimizing the replacement for K-wires[30].

Chapter 2: Formation of Silk Fibroin Thermoplastic - Magnesium Composites

2.1 Introduction

To create these magnesium embedded silk composites, new thermoplastic molds are necessary to achieve the desired rod shape. To compare these newly formulated wires to the current gold standard and other available technologies, certain specifications were required. The gold standard stainless steel K-wires currently used in toe fusion surgery have diameters ranging from 0.9-2.0 mm depending on the patient and their specific case[31]. Other alternatives, like the *ActivaPin,* are available in larger diameters, ranging from 2.0 mm to 2.7 mm. Once machined, the resultant composite pins will aim to have a diameter of about 1.5-2.0mm as to allow for comparison to the current standards. Variation in these diameters may occur as a result of machining inconsistencies.

Novel methods for embedding the magnesium wire into thermoplastics must be optimized prior to the analysis of the 1% SF-Mg composites. This involves creating a system of molds to press the wire directly into the thermoplastic, creating a larger rod with the embedded magnesium wire. This final plastic composite also must be large enough to allow for machining to create the desired end wire shape with the specified diameter[32]. As a result, specific molds must be machined to enable precise embedding of the magnesium wires in the center of the silk thermoplastics. Once this protocol is established, the SF-Mg composites are to be created and further analyzed.

2.2 Materials and Methods

2.2.1 Silk Processing

Silk fibroin solution was prepared from silkworm cocoons according to two established protocols[22,33]. In brief, silk cocoons were degummed via boiling in 0.02 M Na2CO3 for 30 minutes, followed by rinsing in distilled water to remove residual sericin. The degummed silk fibers were then allowed to dry in a fume hood. Subsequently, the silk was dissolved in 9.3M lithium bromide (LiBr) (Sigma-Aldrich) solution at 60 ºC for 4 hours followed by dialysis (MWCO 3,500) of the solution against distilled water for 3 days with 6 changes of water total. After dialysis, the solution was centrifuged at 9,780 x g for 20 min twice to remove any insoluble

impurities. The concentration of the final silk solution was adjusted to be 1 wt/wt %. The solution was then frozen and lyophilized for 5 days or until dried. The resultant dried silk fibroin was then milled into a powder.

2.2.2 Mold Design and Manufacturing

A system of a single base mold and three varying top molds were created to produce silk thermoplastics with the embedded 0.5 mm Mg wire. The molding system was fabricated by the Tufts University machine shop according to the given specifications. The system of top molds aims to place and hold the embedded Mg wire in place throughout the thermopressing process. The protrusion of the first mold of the system, (*Figure 3 (A)*), has an attached metal piece matching the dimensions of the Mg wire. The goal of this piece is to make an indent in the first half of the packed silk powder as to establish the location of the wire in the middle of the thermoplastic. The protrusion of the second mold, (*Figure 3 (B))*, has an indent at the bottom with the dimensions of the wire. As the second half of the silk is added to the mold reservoir, this top piece is used to not only hold the wire in place as to ensure it remains in the center, but also to pack the silk powder surrounding the wire. The protrusion of the last mold, *(Figure 3 (C)),* has a flat bottom as to press the entire system together. This molding system is shown below in Figure 3.

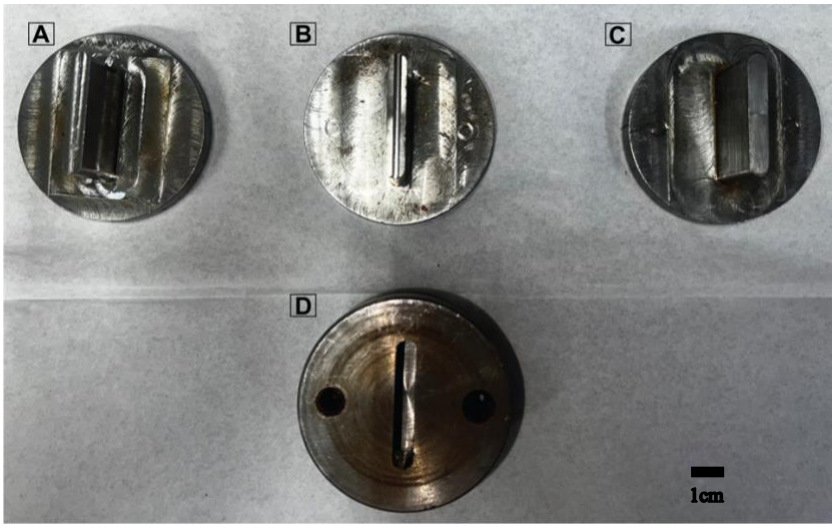

Figure 3. ***Thermoplastic Molding System. (A)*** *First top of the mold system with an attached metal portion on the protrusion, matching the dimensions of the Mg wire.* ***(B)*** *Second top of the system with an indent at the bottom of the protrusion matching the dimensions of the wire.* ***(C)*** *Third top of the system with a flat surface on the protrusion* ***(D)*** *Base of the mold system with a reservoir for the packed silk.*

2.2.3 Silk Fibroin - Magnesium Composite Thermopressing Protocol

A volume of 850 mg of silk was established as being the volume necessary to create a rod with a thickness of about 4.3 mm. This larger diameter was necessary so that the rod can be shaped by the machine shop using the lather to create the desired final wire diameter of about 1.5-2.0 mm.

Half of the total 850 mg volume, 425 mg, is added and packed into the reservoir of the bottom mold. An indent is made into the packed silk powder using the first top piece to indicate the location of the Mg rod in the center of the reservoir. The Mg rod is straightened utilizing a custom 3D printed wire straightener and placed in the center. It is pushed down with the second and third top pieces to ensure it is fixed into place. The second half of the silk, 425 mg, is added and packed into place utilizing the second top piece to ensure the rod is not pushed out of its center position. The third flat top piece is placed on top, and the mold system is inserted into the thermopress between the two heated plates.

In order to achieve a strong thermoplastic material capable of handling loading and other stresses, a temperature of 145°C is necessary as evidenced by a previous paper which has been used to guide the use of thermoplastics throughout this project [34]. As such, the silk-loaded mold is pressed at 300 psi, 145°C, for 15 minutes. Once removed from the thermopress, the thermoplastic cools and is brought to the machine shop where it is shaped using a CNC lathe (Trak TRL 1440 EX, Southwestern Industries) to its final desired diameter of 1.5 mm.

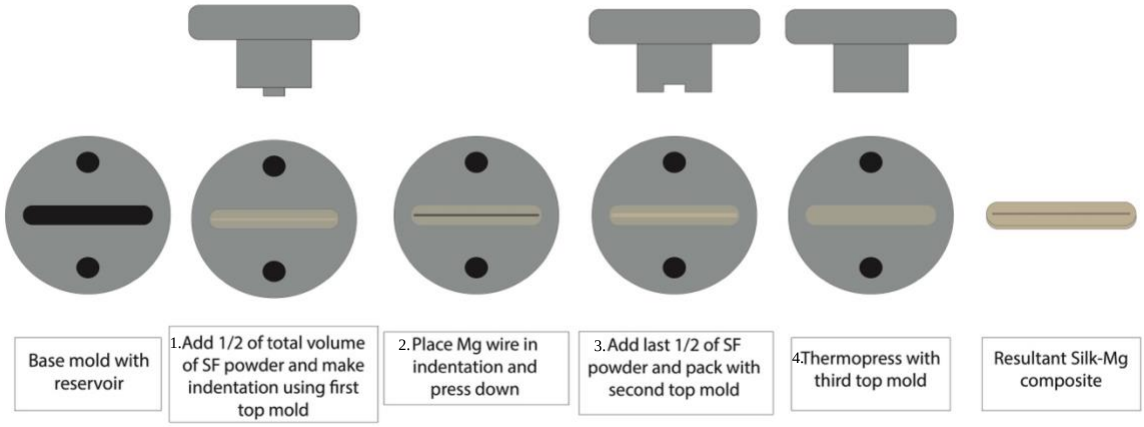

Figure 4. ***Silk-Mg thermoplastic molding protocol.*** *Step 1, the first half of the total volume of silk is packed into the base mold and an indentation is made utilizing one of the specially designed tops to mark the position of the Mg wire in the middle of the packed SF. Step 2, the Mg wire is placed in the indentation and is pressed down to fit into place. Step 3, the last half of the silk is added and packed into place utilizing the second specialized top. Step 4, the packed silk in the mold is then pressed at 300 psi, 145°C, for 15 minutes utilizing the third top. After such time, the resultant composite consists of the SF on the outside with the 0.5 mm embedded Mg affixed in the middle.*

2.3 Discussion and Conclusions

2.3.1 Difficulties Experienced with the Creation of the Silk Fibroin - Magnesium Composite

Although the creation of these silk plastics embedded with Mg proved to be successful, some drawbacks exist. Despite the precise application of the embedded Mg wire in the center of the plastic rod, it proved to be difficult keeping the Mg wire in the middle when turning the plastic rod down to a diameter of about 2 mm. This is attributed to the machinist experiencing difficulty with visualizing the wire during the turning process making it harder to keep the wire in the middle. As a result, some samples had exposed Mg wire, or the wire was not in the middle as it was supposed to be. In the future, improved machining practices such as more precise turning would allow for more consistent and uniform samples. In addition, creating a new molding system that does not require the use of a lathe would be advantageous to prevent any consistencies seen with machining.

Chapter 3: Hydrophobic Coatings to Prevent Water Infiltration

3.1 Introduction

Given the aqueous environment of the human body, preventing premature degradation of the magnesium as a result of corrosion is necessary. To provide ideal mechanical support, allowing for the bone to fuse appropriately, a hydrophobic coating must be identified and used to prevent water infiltration and premature degradation of the Mg wire[26]. Hydrophobic coatings were investigated in an effort to identify the best fit for the given application[27]. Two hydrophobic coatings were chosen Poly (lactic-co-glycolic acid) (PLGA) and Cutin. PLGA is a popular hydrophobic polymer which has been previously used as a coating for magnesium, utilizing the dip coating method[35].

The plant cuticle is a hydrophobic barrier membrane found primarily on the leaf surface. This polymer exhibits remarkable water barrier properties which can be primarily attributed to the hydrophobic polymer material, Cutin [32]. However, Cutin is not commercially available. 16-hydroxyhexadecanoic acid, HHA, or juniperic acid is a naturally derived hydroxy acid which exists in walls of plant cells and is a key monomer of Cutin in the plant cuticle[28,36]. As such HHA will be purchased and polymerized to create PHHA, or a Cutin inspired bio polyester. Throughout the paper, this will be referred to as Cutin. All magnesium wires were prepped via surface roughening to allow for greater adhesion between the coating and the wire surface. The imaging method, AFM will be used to visualize the surface treatment and hydrophobic coatings.

3.2 Materials and Methods

3.2.1 Magnesium Wire Pretreatment

Pure Mg wires (diameter of 0.5 mm and 99.9% purity) were sourced from Sigma Aldrich, St. Louis MO. All Mg wires used were prepped utilizing a series of steps. Prior to use, the Mg wires were polished via 1000 grit waterproof abrasive paper. The wires were then ultrasonically cleaned in acetone and pure ethanol for 20 min to remove any residual contaminants. Finally, they were rinsed with pure ethanol and dried via nitrogen gas flow prior to use[37].

3.2.2 HHA Polymerization

A 98% 16-hydroxyhexadecanoic acid (HHA) was sourced from Sigma Aldrich, St. Louis MO. 2g of HHA powder was placed in a 150°C oven for 24 hours [32]. Upon removal from the oven, the Cutin is a viscous liquid. As it cools to room temperature, the resultant solid is a yellow wax-like substance. This substance can be melted and used to dip coat the magnesium wires.

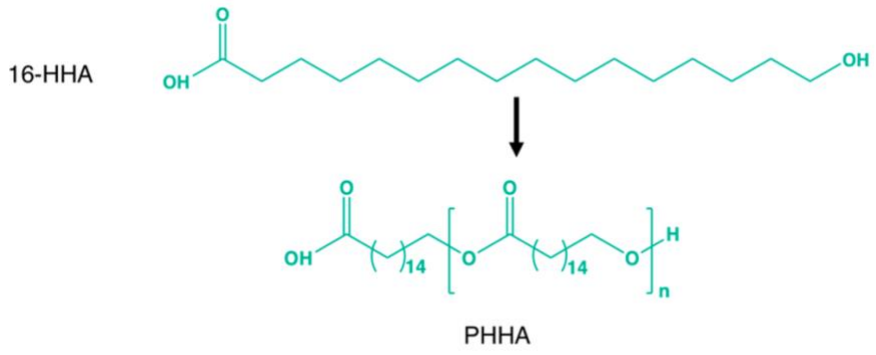

Figure 5. ***Synthesis of Cutin-inspired Poly(hydroxyhexadecanoate) (PHHA) by Melt Polycondensation*** [32] *A structural change can be seen after the polymerization process where the linear 16-HHA becomes a more branched PHHA. This increase in branching results in a more hydrophobic polymer.*

3.2.3 Polymer Preparation and Dip Coating

PLGA (molecular weight *M*W = 66,000-107,000 Da, co-polymer ratio = 90:10) was sourced from Sigma Aldrich, St. Louis MO. A 4.0 wt% PLGA solution for dip coating was prepared by dissolving PLGA powder in acetone[35]. About 12 g of HHA powder was required for polymerization to acquire a volume of about 6.6 ml of Cutin. This volume was necessary for dip coating using a VWR short form glass vial.

Using an Ossila dip coater, the pretreated Mg wires were then immersed into the respective polymer solution at a rate of 10 mm/min and were subsequently slowly withdrawn from the solution at the same rate to obtain a smooth wet layer of polymer solution on the Mg substrates. After 1 hour of hang-drying, the Mg wires were inverted, and their uncoated sides were treated in the same way, resulting in fully coated samples. After full drying, Mg wires were placed in a vacuum oven (-20 Hg) for 12 h at room temperature.[37,38]. AFM was used to confirm and visualize the coating.

3.3.4 Atomic Force Microscopy (AFM)

AFM was performed using a Bruker company Dimension Machine. The parameters for the images were an area of about 30x30 microns, Tapping mode 256 x 256 lines, with a resolution of about 2 nm.

3.3.5 Fourier Transform Infrared Spectroscopy (FTIR)

FTIR was performed using a JASCO FTIR 6200 spectrometer (FT/IR-6200, JASCO) equipped with a MIRacle attenuated total reflectance Ge crystal cell in absorbance mode.

3.4 Results

3.4.1 AFM imaging of Coated Mg surface

Visualization of the coated surface of the Mg wires was required in order to confirm deposition of the coating and evaluate uniformity. The visualization of the Mg surface was performed via AFM and the results are shown below in Figure 6.

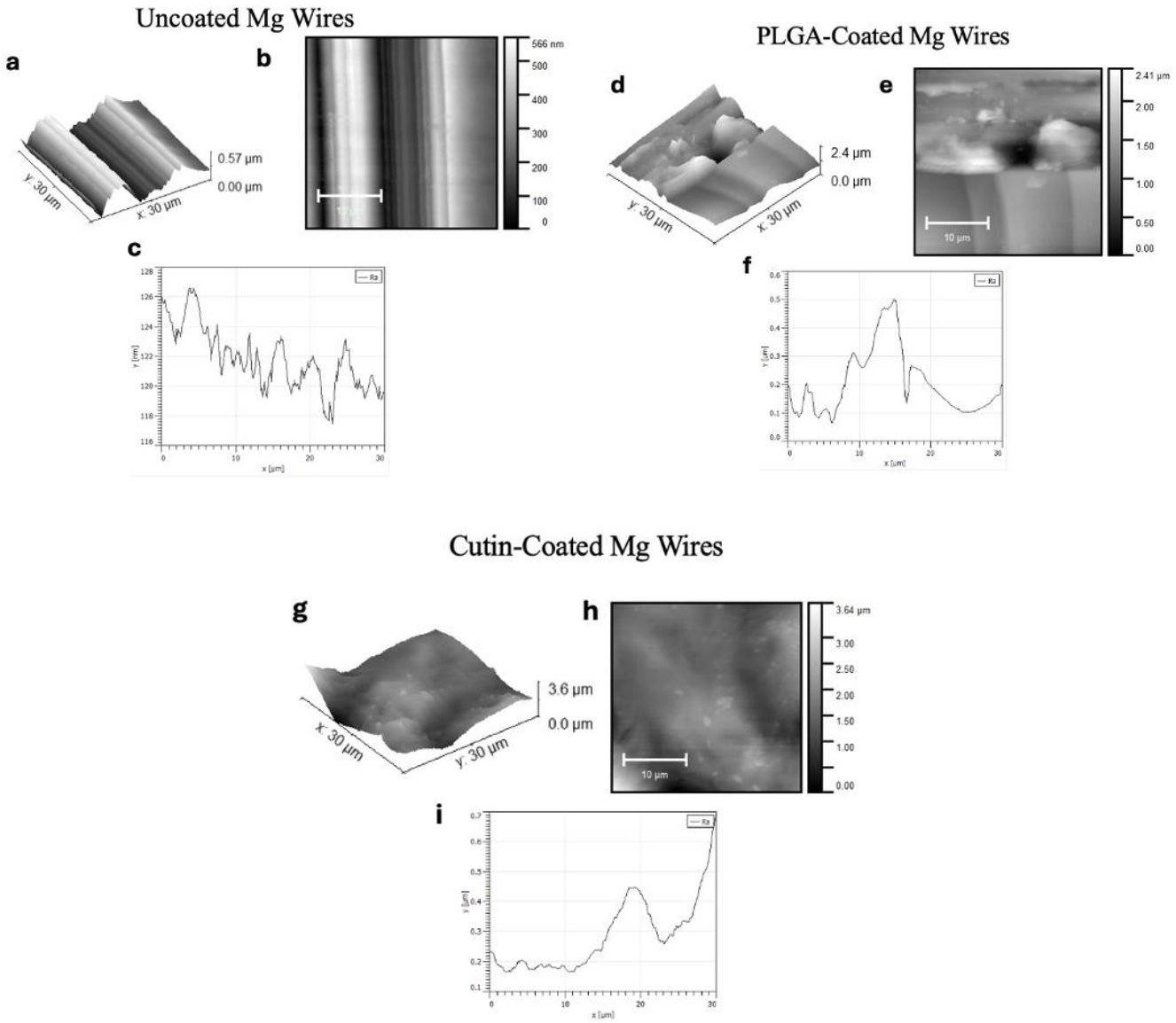

Figure 6. ***AFM imaging of Coated Mg wires. (a-c)*** *AFM images of uncoated Mg wire****. (d-f)*** *AFM images of PLGA-coated Mg wire.* ***(g-i)*** *AFM images of Cutin-coated Mg wire****. (a, d, g)*** *Topographic map of the wire surface, (30 µm x* 30 *µm*). ***(b, e, h)*** *Cross sectional area image of the wire's surface. The scale bars are 10 µm for all three images.* ***(c, f, i)*** *Average roughness graphs (RA) depicting the roughness of the surface of the wire. Both the x and y axis are measured in microns (µm).*

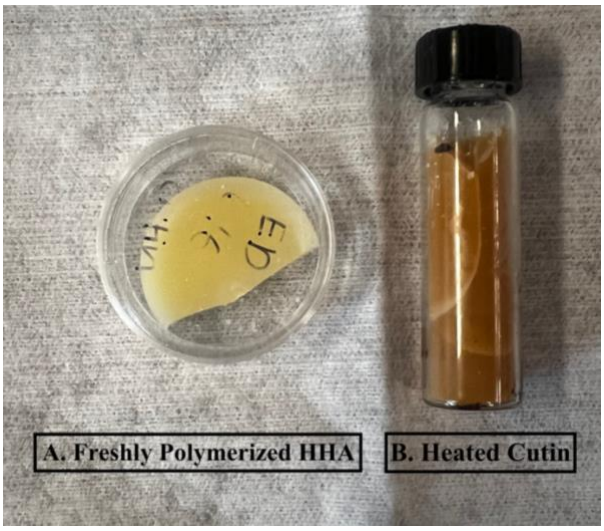

Figure 7. ***Post Polymerization of Cutin (A)*** *A yellow solid. Freshly polymerized HHA(Cutin) which has not been subject to heating via heat plate.* ***(B)*** *An orange solid. Polymerized HHA (Cutin) which has been repeatedly heated using a hot plate for dip coating and as a result, the color changed.*

3.4.2 FTIR Spectroscopy analysis of Cutin

In order to properly dip coat the Mg wires utilizing liquid Cutin, repeated heating of the Cutin was necessary. While using a hot plate to melt the Cutin, a color change occurred. The Cutin changed from a light yellow to darker orange color indicating the potential for some functional group changes and subsequent structural alterations. This color change can be seen above in Figure 7. Given time constraints, the darker colored Cutin was to be used for dip coating and subsequent sample formulation. To better understand whether any significant structural changes occurred as a result of heating, FTIR analysis was performed.

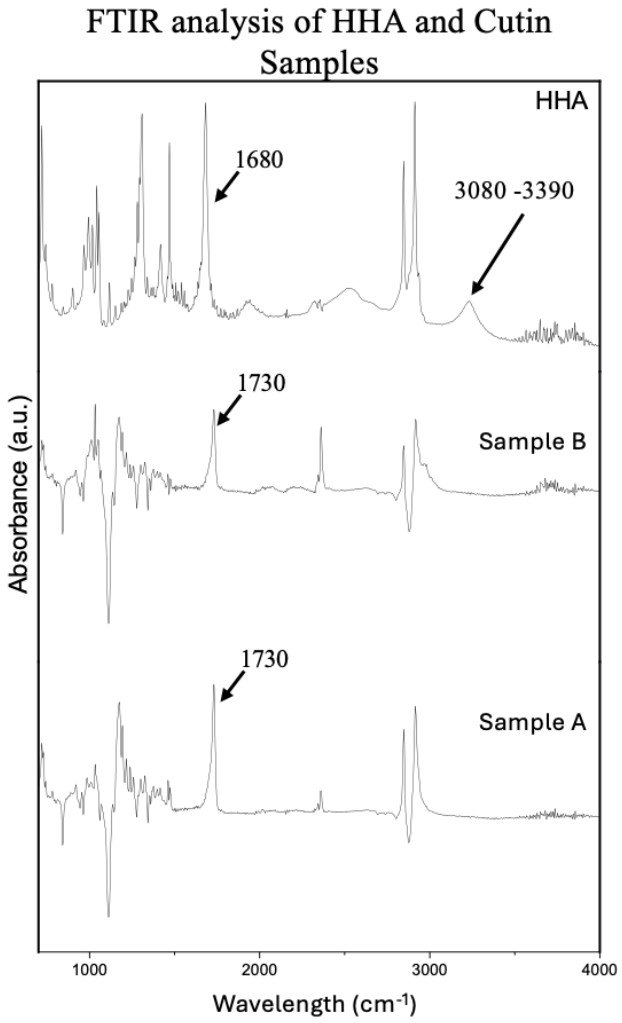

Figure 8. ***FTIR Spectra of HHA, freshly polymerized Cutin, and repeatedly heated Cutin.*** *Sample A represents the freshly polymerized Cutin which exhibits a lighter yellow color. Sample B represents the Cutin which exhibits a darker orange color as a result of repeated heating. HHA is the key monomer in Cutin and represents both Sample A and B prior to the polymerization process. Comparison of HHA to both sample A and B can indicate whether Cutin was properly formed. Comparison of sample A and B can indicate whether any structural changes occurred as a result of repeated heating.*

3.4.3 FTIR results

In Figure 8 above, sample A represents the spectra of freshly polymerized Cutin, and sample B represents the spectra of Cutin which has been subjected to repeated heating. Both samples exhibited the same peak position but differed in the intensity of these peaks. More specifically, the peaks in sample B exhibited more intense peaks as compared to sample A. The synthesized Cutin polymer in both samples A and B can be confirmed by the appearance of the 1730 cm^{-1} peak. According to previous literature, this can be attributed to stretching of the ester C=O. This is also supported by the disappearance of the 3080-3390 and 1680 cm^{-1} bands in the HHA spectra, indicating that most hydroxyl groups were consumed during the esterification reaction to produce the polyester.

3.5 Discussion and Conclusions

Coating of the hydrophobic polymers on the prepped Mg wires was proven via AFM. The coated 0.5 mm Mg wires that were used in the composites proved to be too small to be visualized via AFM. As such, 1.0 mm Mg wires were coated and used to confirm coating via AFM. Figure 6 shows the results of AFM imaging of the uncoated, PLGA-coated, and Cutin-coated Mg wires. It can be seen that the uncoated and Cutin-coated images confirmed successful coating. However, the PLGA AFM images showed inconsistent coating. More specifically, in Figure 6(e) a clear line can be seen. The top portion shows the polymer coating as indicated by its structure while the bottom portion resembles the uncoated wire shown in Figure 6(b). The black holes indicate gaps in the coating and polishing lines can also be seen. This indicates a non-uniform coating on the PLGA-coated wires.

Figure 6(h) proves the successful coating of Cutin as the polymer structure can be identified on the surface. Given the high viscosity of Cutin, coating was found to be easier and more cohesive as opposed to PLGA. In addition, higher molecular weight PLGA was supposed to be used for coating to allow for a prolonged degradation process. However, the higher molecular weight, 140,000 Da, PLGA was unavailable and as such, a lower molecular weight PLGA,66,000-107,000 Da was used at a 4% concentration. This, in addition to the parameters of dip coating could have contributed to the inconsistent coating.

A high roughness can also be identified on the surface of the wires shown in Figure 6 (a, d, and g). This is confirmed by the graphs shown in Figure 6 (c, f, i). The average roughness was

121.8 ±2.053 nm for uncoated, 205.4 ± 114 for PLGA-coated, and 285 ± 116.2 nm for Cutin-coated. This high surface roughness can result in the roughened portions being superior to the coating, preventing full coverage.

Moving forward, several factors should be adjusted. Specifically, a higher molecular weight PLGA should be used as well as altered dip coating speeds and associated parameters to produce a thicker coating of about 1-100 μm[39]. Additionally, a standardized roughening method should be established to create less roughness and produce more consistent and thick coatings[32].

The evidence presented in Figure 8 indicates the successful formulation of PHHA or Cutin as proven by the appearance of the 1730 cm^{-1} peak in addition to the disappearance of the 3080-3390 and 1680 cm^{-1}. As such, this confirms both sample A and B were successfully polymerized into Cutin. The repeated heating of the Cutin proved no significant structural changes except for slightly lowered intensity of the spectra compared to the freshly polymerized Cutin.

Chapter 4: In Vitro Protease XIV Enzymatic Degradation Study

4.1 Introduction

Degradation studies are to be performed to ensure the composite wires are capable of following the desired degradation timeline to allow for appropriate bone fusion and provide the necessary mechanical support throughout the healing process. The evaluation of these wires aims to provide an advanced understanding of both their performance and stability.

4.2 Materials and Methods

PLGA and HHA coated Mg composites were tested, in addition to uncoated Mg composites and, pure silk wires. For the in vitro degradation of the composite wires, machined 1% SF-Mg wires ($n = 3$) were incubated at 37 °C in PBS solution and 5 U ml^{-1} protease XIV (Sigma-Aldrich) PBS solution, respectively. For each wire, 4 mL of incubation solution was used. The incubation solutions were changed every 2–3 days. At each solution change throughout the 4 weeks the samples were rinsed in deionized water and dried for 2 hours before weighing. The remaining mass of each sample was recorded [34].

4.2.1 Calculations

$$\boldsymbol{Residue\ Mass\ Ratio}\ (\%) = \frac{\boldsymbol{day\ x}}{\boldsymbol{day\ 0}} * \mathbf{100} \quad (22)$$

4.3 Results

The 1% SF samples degradation behavior was consistent with that of previous literature. The 1% SF samples in protease XIV samples indicated slow and minimal degradation with a residual mass ratio of about 80%. The previous literature presented a residual mass ratio of 85% for 1% SF samples prepared at 145 °C. The 1% SF sample incubated in PBS showed little to no degradation and a residual mass ratio of 100% which is consistent with the results of previous literature. Some discrepancies did occur which resulted in the exclusion of a few samples which will be discussed further. At day 30, warping of the wires into a half-bent shape was observed in PLGA-coated, uncoated, and 1% SF samples in both protease and PBS solutions, just PBS, and just protease solutions, respectively. Overall, the samples placed in the protease XIV solution

showed faster degradation as compared to those incubated in PBS, which is consistent with previous hypothesis.

4.3.1 Protease XIV Degradation Results

Both coated samples, PLGA and Cutin-coated, exhibited similar behavior in protease XIV solution, with a faster degradation ending with a residual mass ratio of 40% as compared to the 1% SF and uncoated samples. The Cutin only began to degrade on day 10 whereas the PLGA decreased steadily starting from day 0. The uncoated samples had a steady degradation as well ending with a residual mass ratio of 60%. The 1% SF samples indicated minimal degradation resulting in a residual mass ratio of 80% which closely matched the results from literature as mentioned previously. A one-way ANOVA test indicated a significant difference between the 1% SF samples and the Cutin-coated samples with a p-value of 0.0281. In addition, a significant difference was identified between 1% SF samples and PLGA-coated samples with a p-value of 0.0073.

4.3.2 PBS Degradation Results

Samples placed in PBS indicated consistent behavior with minimal degradation. The 1% SF and uncoated sample's residual mass ratios did not fall below 100% whereas the Cutin and PLGA-coated samples fell slightly under 100%. The behavior of the 1% SF samples in PBS was consistent with previous literature. Throughout the 30 days, the samples exhibited residual mass ratios above 100% which could be attributed to some error. Overall, the samples degradation behavior was consistent and exhibited little to no degradation.

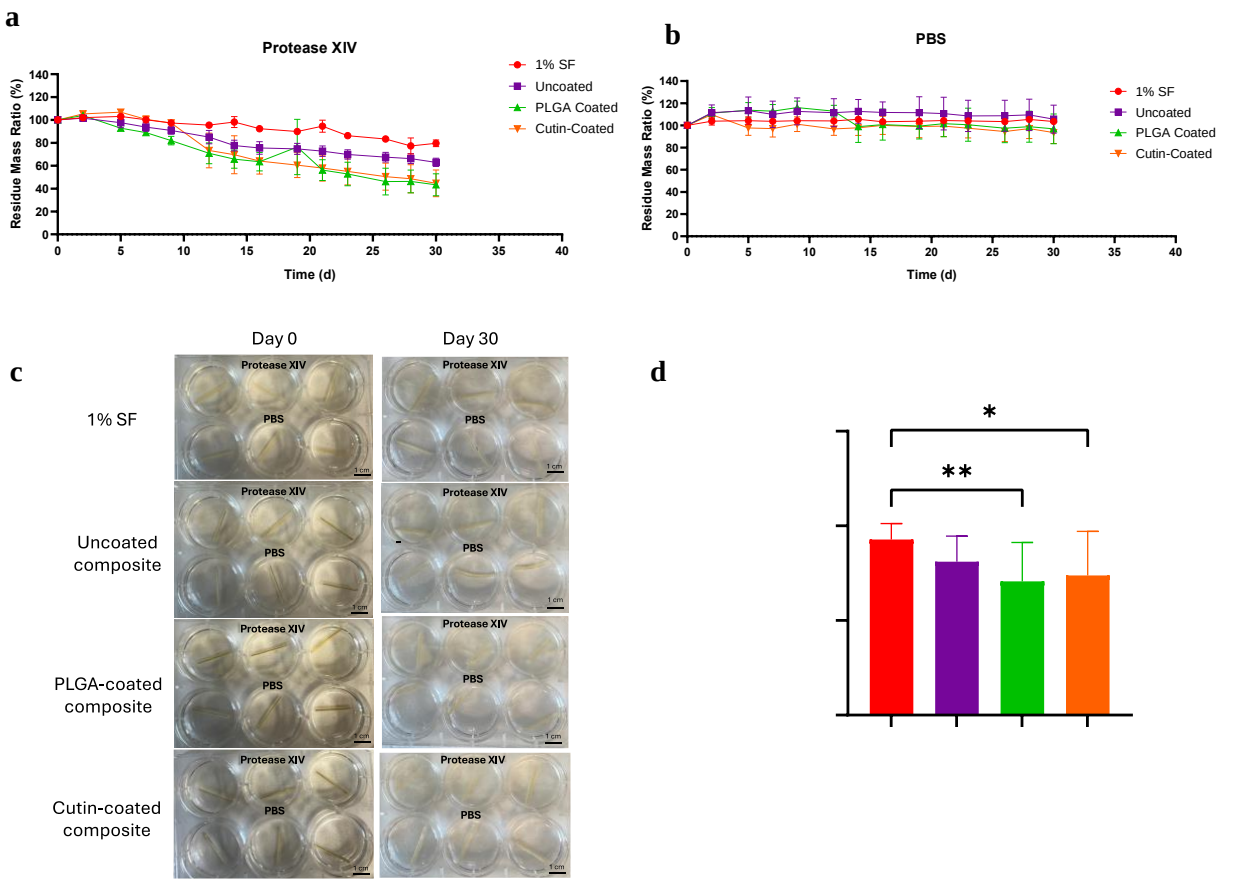

Figure 9. ***In vitro testing of SF-Mg composite wires. (a-b)*** *In vitro degradation profiles of SF-Mg composite wires in solution* ***(a)*** *protease XIV (5 U/ml^{-1}) PBS solution* ***(b)*** *and 1X DPBS.* ***(c-d),*** *In vitro degradation analysis of composites with varying Mg coatings.* ***(c)*** *Photographs of the SF-Mg composites incubated in protease XIV (top row) and PBS (bottom row) at 37 °C at day 0 and day 30.* ***(d)*** *Residual mass ratios of the SF-Mg composite wires over 30 days. A one-way ANOVA with a Tukey-Kramer post-hoc test was used to analyze these data, *p<0.05, **p<0.01, Error bars, SD, n=3 per group.*

4.4 Discussion and Conclusions

The initial hypothesis indicated that the coated samples were expected to exhibit similar behavior as the 1% SF samples since the role of protease is to break down the silk proteins. However, since the coated samples contained the magnesium wire, this disrupted the overall structure of the composite, allowing for easier infiltration of the protease solution and as such, a faster degradation. This can be seen in Figure 10 where a PLGA sample is split in half as a result of the embedded wire. This theory is supported by the data as a significant difference was identified between the 1% SF samples and the coated samples. No significant differences were identified between the coated and uncoated samples which suggests the coating does not

influence the degradation of the silk protein, as expected. Moving forward, improving the interactions between the coated wires and the silk is essential to allow for a long lasting and cohesive wire.

Despite these factors, the wires were able to withstand 30 days in solution while losing only about half of their mass. Arthrodesis surgery of the toe requires a timeline of about 2-3 months depending on the patient. Given the established timeline, the samples should be capable of holding the toe in place to allow for full fusion over the given time period. After the surrounding silk degrades, the magnesium wire will be capable of holding the joints in place allowing for full fusion and subsequent healing. A longer degradation study would allow for a greater understanding of the role of the coatings and the long-term behavior of the composites. Utilizing simulated body fluid or Hank's solution may also help to understand the composites behavior in a different solution [40] .

The warping of the samples could be attributed to the sample formulation. Given the softness of the magnesium wire, this change in shape is possible. However, with the replacement of the Mg wire with an alloy, this can increase the strength of the composite as a whole preventing any kind of shape change.

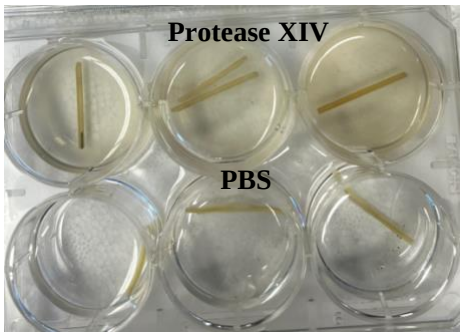

Figure 10. ***PLGA Degradation study, Day 19****. Day 19, PLGA sample 2 in protease split in two separate pieces as a result of the embedded Mg wire. This could account for the faster degradation times of the composite samples seen in the data.*

4.4.1 Contamination and other Potential Errors

Throughout the degradation study some error occurred which could have influenced the results. Firstly, although the samples placed in PBS were consistent and followed the same trendline, many of their residual mass ratios were calculated to be above 100%. This can likely be attributed to the samples not being fully dried prior to weighing. Considering that the samples

consisted of multiple components, longer drying time may be required to ensure that the samples are fully dry prior to weighing.

Some contamination occurred during the study which led to inconsistent data. A white like growth was identified on two samples and as such, those samples were excluded from the data. Specifically, PLGA-coated wire sample 5 in PBS was excluded as a result of some kind of contamination as can be seen in Figure 11 (a). Cutin-coated wire sample 1 in Protease was also excluded as a result of contamination which can be seen in Figure 11(b).

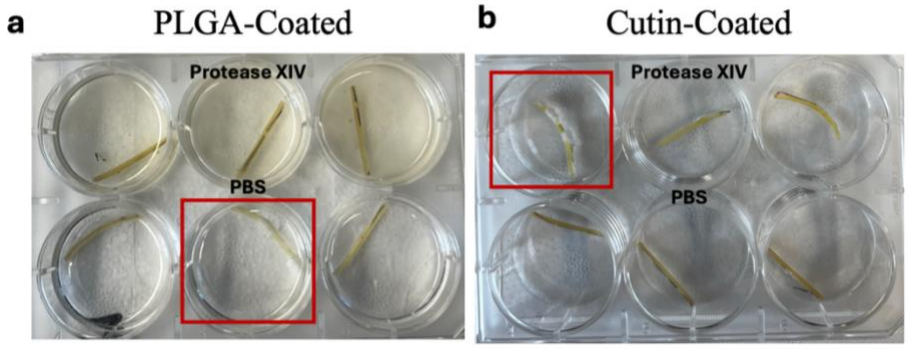

Figure 11. ***Excluded Samples in the Degradation Study. (a)*** *Day 2, PLGA sample 5 in PBS, shown in the red box, portrays a white substance attached to the wire, indicating contamination.* ***(b)*** *Day 2, Cutin sample 1 in protease XIV, shown in the red box portrays a white substance on the wire, indicating contamination. As a result of this contamination, these samples were excluded from the data.*

Chapter 5: Mechanical Evaluation of Composite Wires

5.1 Introduction

The composites must be evaluated to ensure they are capable of meeting the mechanical requirements of bone without causing stress shielding or falling below the necessary mechanical strength. The mechanical strength values of both native bone and current K-wires were collected for comparison[29]. Three-point bending tests were performed on the composites in both dry and hydrated states.

5.1.1 Tensile Testing of SF-Mg Composite Wires

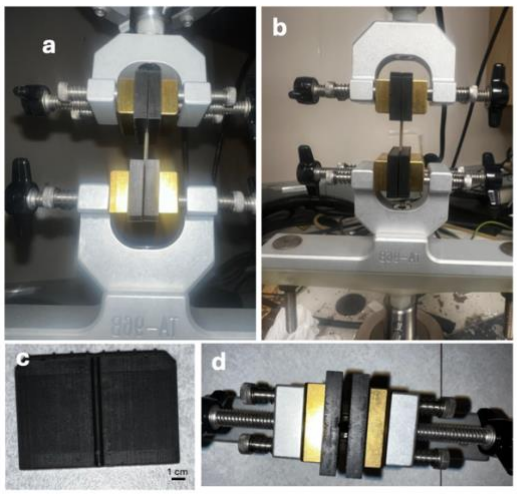

Figure 12. ***Custom Clamping System for Tensile Testing. (a, b)*** *Tensile testing with clamps and inserted SF-Mg composite wire.* ***(c)*** *Custom printed clamp covers with indent matching the diameter of the composite wires.* ***(d)*** *Close up of the custom clamp covers over the existing clamps.*

Given the small size and circular geometry of the composite plastic wires, smaller clamps were required to sufficiently hold either end of the sample for tensile testing. To circumvent this problem, clamps meant for a texture analyzer (TA. XTPlus 100 Connect, Texture Technologies Corp.) were used. These clamps were far smaller than the Instron tension testing clamps, allowing for a better grasp on the samples. Adapter pieces were 3D printed to allow for a connection between the texture analyzer clamps and the Instron. Despite utilizing these new clamps, the sample continued to demonstrate slipping during testing.

To bypass this additional issue, 3D printed plastic covers were printed which have a 2mm indent running through them to better grasp the 2 mm samples for testing. This adjustment did

indicate improvement in slipping of the samples as compared to the previous two designs. The clamping system is shown in Figure 12. One potential problem with this indent involved variation in the sample diameters so not all samples fit exactly into the 2 mm indent. This problem can be attributed to a machining inconsistency. Because of this, the slipping persisted causing inaccurate and inconsistent data. Given the time constraints to complete the project, three-point bending was determined to be the best method for mechanical analysis.

In the future, to potentially circumvent this last portion of slipping of the sample, the 3D printed plastic covers could be roughened to create a texture, allowing for better adhesion between the surface and the sample. In addition, instead of creating an indent matching the dimensions of the sample, a V shape could be utilized to affix the sample in place, avoiding the need for consistent 2 mm diameter samples.

5.2 Materials and Methods

5.2.1 Three-Point Bending of Silk-Mg thermoplastic wires

Mechanical testing of the silk-Mg thermoplastic wires followed mechanical testing protocols from an associated paper [34]. The three-point bending tests were performed on an Instron 3366 machine in flexural test mode with a loading rate of 0.2 mm min^{-1} or 2 mm min^{-1} for dry specimens and wet specimens, respectively. The dry specimens had an average length of 23.8 mm and an average diameter of 1.4 mm for all tests. The wet specimens were soaked in 1x DPBS for 24 hours and incubated at 37 °C prior to testing. Length and diameter measurements were taken before and after hydration. Prior to hydration, the dry samples had an average length of 24.5 mm and an average diameter of 1.4 mm. After hydration, the samples had an average length of 26.5 mm and an average diameter of 1.6 mm. The average change in sample length after hydration was +2 mm and the change in diameter was +0.15 mm. Multiple samples (n=3) were tested for each condition.

Tables 2-5 below portrays the specifications of each independent sample. The samples exhibited some imperfections involving the wire not being centered and close to the edge of the sample in addition to some wire exposure. This is largely attributed to inconsistencies with machining. Moving forward, alternative machining practices should be explored to create more consistent samples.

Table 1. ***1% SF wire and flat bar composite samples specifications for 3-pt bending***

1% SF						
	Sample 1- DRY **Wire**/ Flat Bar	Sample 2- DRY **Wire**/ Flat Bar	Sample 3- DRY **Wire**/ Flat Bar	Sample 1- HYDRATED	Sample 2- HYDRATED	Sample 3- HYDRATED
Initial Diameter	**1.5** / 2.1 mm	**1.5**/ 2.1 mm	**1.3**/ 2 mm	1.4 mm	1.4 mm	1.4 mm
Final Diameter	-	-	-	1.7 mm	1.6 mm	1.5 mm
Initial Length	**25.2**/ 30 mm	**24.8**/ 30 mm	**24.7**/29.8 mm	23.8 mm	24.7 mm	24.3 mm
Final Length	-	-	-	26.0 mm	26.6 mm	25.9 mm

*Table 2.****Uncoated wire and flat bar composite sample specifications for 3 pt-bending***

Uncoated						
	Sample 1- DRY **Wire**/ Flat Bar	Sample 2- DRY **Wire**/ Flat Bar	Sample 3- DRY **Wire**/ Flat Bar	Sample 1- HYDRATED	Sample 2- HYDRATED	Sample 3- HYDRATED
Initial Diameter	**1.4**/ 2 mm	**1.6**/ 2 mm	**1.3**/ 2.3 mm	1.5 mm	1.5 mm	1.5 mm
Final Diameter	-	-	-	1.4 mm	1.6 mm	1.5 mm
Initial Length	**25.2**/ 30 mm	**25.4**/29.9 mm	**20.7**/ 29.9 mm	25.6 mm	25.2 mm	24.4 mm
Final Length	-	-	-	26.8 mm	26.6 mm	25.9 mm

Table 3. ***PLGA-coated wire and flat bar composite sample specifications for 3 pt-bending***

PLGA-Coated						
	Sample 1-DRY **Wire**/ Flat Bar	Sample 2-DRY **Wire**/ Flat Bar	Sample 3-DRY **Wire**/ Flat Bar	Sample 1-HYDRATED	Sample 2-HYDRATED	Sample 3-HYDRATED
Initial Diameter	**1.3**/ 2 mm	**1.3**/ 2 mm	**1.3**/ 1.9 mm	1.4 mm	1.4 mm	1.4 mm
Final Diameter	-	-	-	1.5 mm	1.6 mm	1.4 mm
Initial Length	**21.7**/ 29.8 mm	**25.0**/ 29.9 mm	**24.7**/ 29.9 mm	25.3 mm	22.9 mm	23.0 mm
Final Length	-	-	-	27.6 mm	25.2 mm	25.2 mm

Table 4. ***Cutin-coated wire and flat bar composite sample specifications for 3 pt-bending***

Cutin-Coated						
	Sample 1-DRY **Wire**/ Flat Bar	Sample 2-DRY **Wire**/ Flat Bar	Sample 3-DRY **Wire**/ Flat Bar	Sample 1-HYDRATED	Sample 2-HYDRATED	Sample 3-HYDRATED
Initial Diameter	**1.4**/ 1.8 mm	**1.3**/ 1.9 mm	**1.3**/ 2 mm	1.5 mm	1.3 mm	1.5 mm
Final Diameter	-	-	-	1.6 mm	1.5 mm	1.7 mm
Initial Length	**24.4**/ 29.9 mm	**18.0**/ 29.5 mm	**25.3**/29.7 mm	25.0 mm	24.2 mm	24.5 mm

Final Length	-	-	-	27.0 mm	25.9 mm	26.8 mm

5.2.2 Calculations

The following equations for flexural stress (σ_f), flexural strain (ϵ_f), and flexural modulus (E_f) were used for samples with a circular cross-section.

$$\sigma_f = \frac{FL}{\pi R^3} \quad (41)$$

$$\epsilon_f = \frac{6Dd}{L^2} \quad (41)$$

$$E_f = \frac{L^3 m}{12\pi R^4} \quad (41)$$

The following equations for flexural stress (σ_f), flexural strain (ϵ_f), and flexural modulus (E_f) were used for samples with a rectangular cross-section.

$$\sigma_f = \frac{3FL}{2bd^2} \quad (42)$$

$$\epsilon_f = \frac{6Dd}{L^2} \quad (41)$$

$$E_f = \frac{L^3 m}{4bd^3} \quad (42)$$

F=load at a given point on the load deflection curve (N), L= Support span (mm), R= radius of the beam (mm), m=the gradient (i.e., slope) of the initial straight-line portion of the load deflection curve (N/mm).

5.3 Results

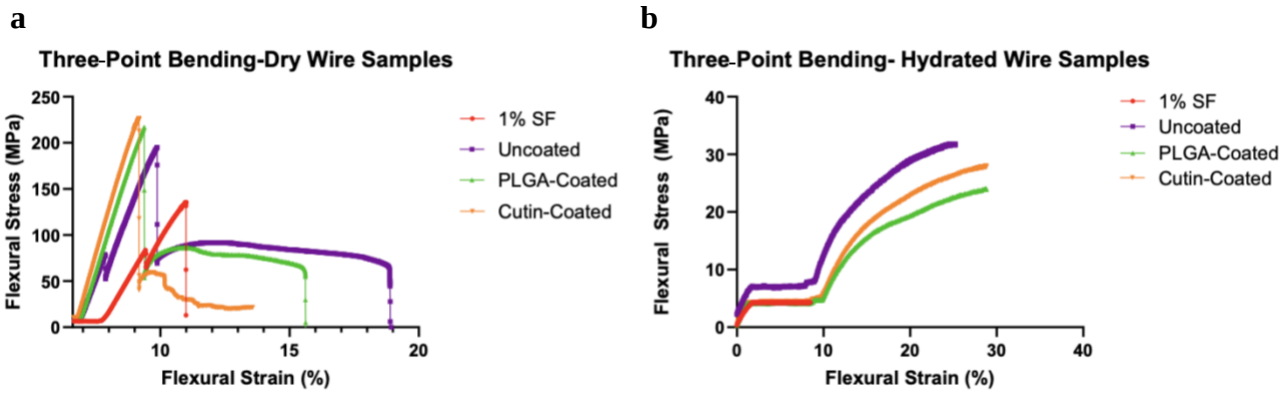

Figure 13. ***Three-Point Bending of Dry and Hydrated Samples. (a)*** *Three-point bending of SF-Mg composite wire samples in dry conditions.* ***(b)*** *Three-point bending of SF-Mg composite wire samples in hydrated conditions, where samples were placed in 1X DPBS for 24 hours prior to testing.*

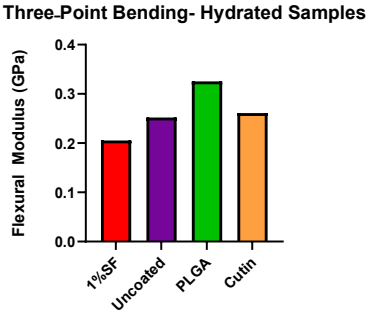

Figure 14. ***Flexural Moduli of Hydrated SF-Mg Wire Samples.*** *Calculated moduli of hydrated 1% SF, Uncoated, PLGA-coated, and Cutin-coated samples after three-point bending testing.*

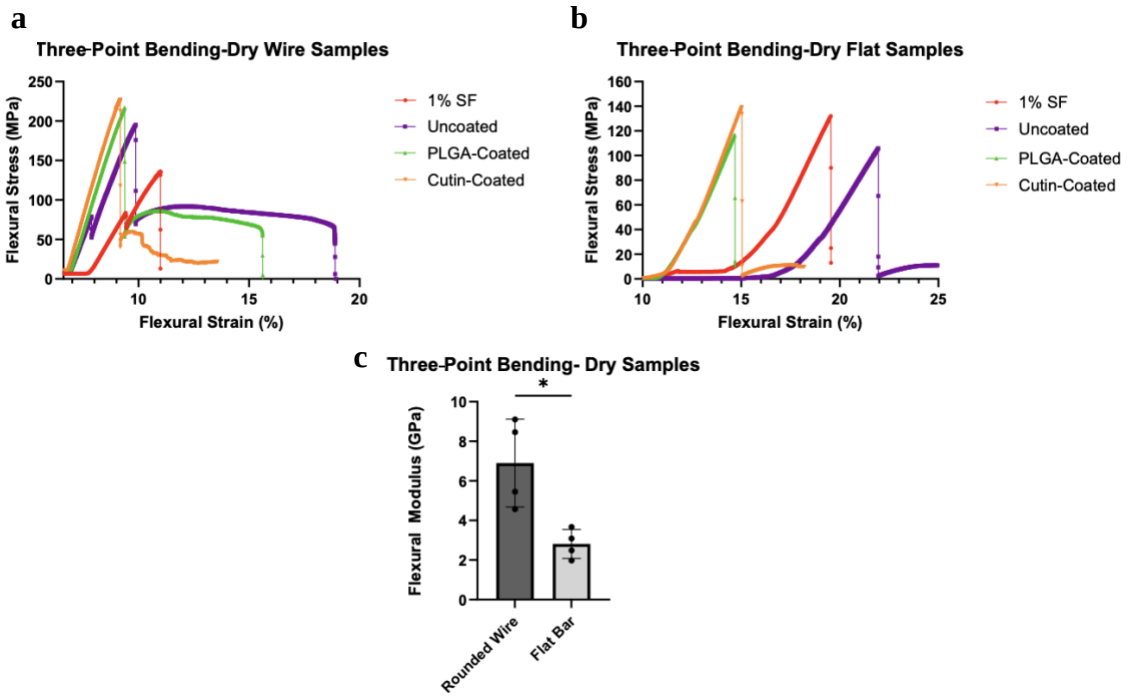

Figure 15. ***Three-Point Bending of Dry Samples with Varying Geometries. (a)*** *Three-point bending of dry SF-Mg rounded wire samples.* ***(b)*** *Three-point bending of dry SF-Mg flat bar samples.* ***(c)*** *Flexural Moduli of the rounded wire and flat bar. An unpaired t- was used to analyze these data, *p<0.05, Error bars, SD, n=3 per group.*

5.4 Discussion

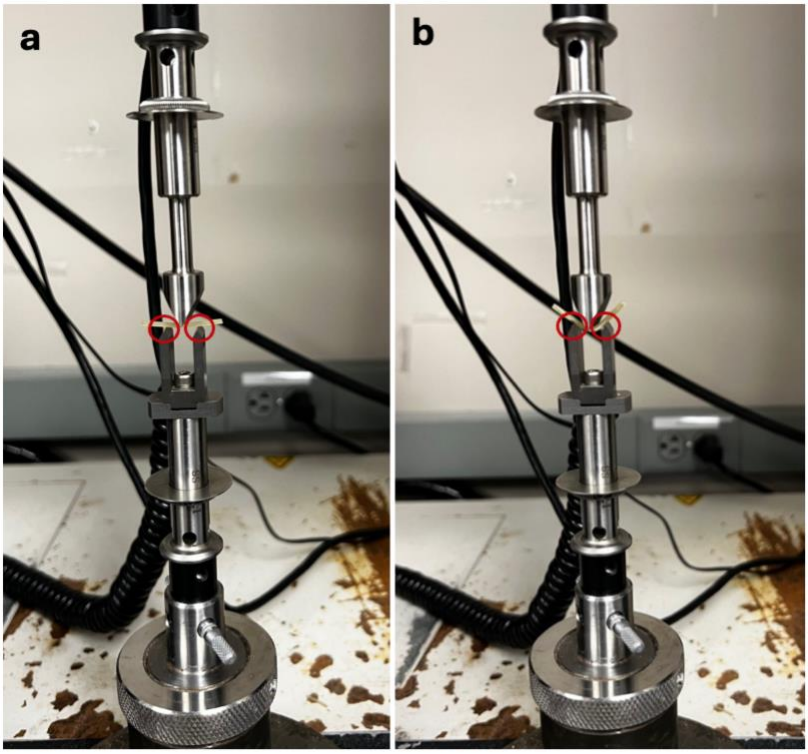

Figure 16. ***Three- point bending testing of uncoated hydrated samples. (a)*** *Initial plunger location prior to the start of testing where the red circles indicate the initial points of contact between the sample and support span.* ***(b)*** *Plunger location at the end of testing where the red circles indicate the final points of contact between the sample and the support spans.*

The graphs shown in Figure 13 highlight the three-point bending results from SF-Mg wires in both dry and hydrated states. The 1% SF samples in dry conditions were found to reach a maximum flexural stress of approximately 225 MPa and failed at a strain of about 7%. This is consistent with the 1% SF samples prepared at 145 °C in previous literature which were found to have a maximum flexural stress of approximately 175 MPa and failed at a strain of about 2.5%[22]. In addition, the failure of the SF portion of the composite can be seen in Figure 15 (a) and (b) followed by the composite being mechanically supported by the embedded Mg until complete failure. As proven by the data, the 1% SF wire samples were capable of handling higher stress however, some errors occurred during testing.

A premature peak can be identified on the graph in Figure 13(a) on both the 1% SF and Uncoated samples. Given the rounded geometry of the samples, it was hypothesized that this was a potential factor in these premature peaks. It's possible the samples were slightly shifting/rolling during testing as this was previously observed. As such, flat samples were created utilizing the

same methods and parameters as the wires. This resulted in flat bars with embedded Mg wires and a thickness of about 2 mm, consistent with the specifications of the wire samples.

In a physiological setting, the geometry of the sample should have negligible effects on the mechanical properties of the composite if the compositions are the same. However, the goal of testing the samples in their final rounded wire form was to allow for a comprehensive evaluation of the composite for the purpose of understanding its performance if it were to be implanted and used for toe fusion. However, in mechanical testing via three-point bending, the geometry does in fact have an influence on the mechanical behavior of the samples as evidenced by the collected data. As such, two different geometries were tested to identify their influence in testing.

As can be seen in Figure 15 (c), the moduli of both flat and rounded samples were found to be between 3 and 7 GPa, consistent with the moduli of brittle materials and the data from the previous paper. Although the flexural modulus for the 1% SF sample was calculated to be 2.5 GPa which is much smaller than the modulus calculated in the paper which was 8 GPa. This could again be attributed to problems associated with the testing of the samples or the silk cocoons that were used to prepare the 1% SF. A significant difference was identified between the moduli of the rounded wire samples and the flat bar samples as indicated by the p-value of 0.015. When testing the flat samples, no premature peaks can be seen in the data, indicating that the shape of the samples could very well be the reason behind this phenomenon.

The flat samples were expected to reach a higher flexural stress given their optimal shape for three-point bending testing. However, the moduli of the rounded wire were found to be higher than the flat bars. This shows that despite the potential for rolling and the premature peaking, the samples were still capable of handling higher stress. The 1% SF samples of both rounded and flat geometries were found to reach about the same flexural stress, 140-150 MPa. Despite this, further studies should be performed, specifically creating a support span which can hold the wire in place throughout testing to prevent any kind of shifting or movement. In theory, creating a half circle shape with a 2 mm diameter in both support spans would ideally hold the sample in place, allowing for the collection of data without movement.

According to literature, phalangeal cortical bone has a longitudinal modulus of 17-20 GPa and a transverse modulus of: 6-13 GPa [43]. Considering the samples reached a max of 7 GPa in dry conditions and 0.35 GPa for hydrated samples, some changes need to be made in order to

improve the mechanical strength of the composites so that they can be successful in holding the toe joints in place of fusion. The gold standard in toe fusion surgery, K-wires, specifically 304 stainless steel wires, have a modulus of elasticity of 193-200 GPa[44]. These values provide guidance as to where the current composite needs to be mechanically in order to be successful in vivo.

After 24 hours in PBS, the hydrated samples became rubber-like and malleable. When tested, the hydrated wire samples exhibited an unexpected mechanical behavior as the data shows an initial linear trend as the samples take on stress. However, the stress then plateaus and once it reaches a strain of about 10% the samples then begin to take on stress again in a more gradual manner. The 1% SF samples also showed this pattern with an initial linear region and then a plateau, but the testing was stopped at 8% strain as consistent with the previous literature. As such it could not be determined whether the 1% SF samples experienced a gradual stress curve as consistent with the other samples. This should be further explored in future studies.

Three-point bending is typically better suited for dry, rectangular samples which could be a large factor contributing to this error. However, this unusual mechanical behavior in the hydrated samples could be explained by the shift in points of contact between the sample and the support spans. Figure 16 highlights this potential problem where the initial points of contact prior to testing can be seen in Figure 16(a) and after testing, the points of contact are seen in Figure 16(b). The initial stress experienced by the sample can likely be attributed to the plunger initially puncturing the hydrated sample. This stress plateaus as the points of contact slip gradually and once they catch and reach their final positions, the samples begins to take on more stress in a gradual manner. To confirm and better understand this phenomenon, hydrated samples should be tested again, and the initial and final points of contact should be marked as to better understand how the sample is shifting. However, The obtained flexural moduli taken from the initial linear region of the samples were found to be between 200-350 MPa, consistent with the previous literature as well as the behavior of elastic materials.

5.5 Conclusion

Given that these data proved the composite wires fell short of the mechanical requirements, potential alternatives should be explored. Magnesium alloys are becoming increasingly popular as they have demonstrated improved mechanical strength and potential to be tailored to specific needs. Specifically, the newly developed Mg-Cu alloys have the potential

to aid in osteogenesis and bone fixation[45,46]. However, these alloys are not currently available, especially medical grade alloys which are necessary for use in the proposed medical device. As such, this project has aimed to demonstrate a proof of concept where the pure magnesium wire may be substituted for a stronger and improved magnesium alloy as they become commercially available.

More mechanical testing with improved fixtures should be conducted to acquire more consistent and accurate data. In addition, oscillatory three-point bending should also be conducted in the future to mimic physiological loading conditions for a more comprehensive understanding of the mechanical behavior.

Chapter 6: Final Conclusions

6.1 Conclusion and Future Directions

Current K-wires and associated alternatives fail to address core drawbacks involving both toe mobility after surgical fixation as well as the need for multiple hospital visits. The proposed SF-Mg composite thermoplastic wire aims to address these concerns by incorporating the native orientation of the patients toe in addition to utilizing biodegradable materials to prevent the need for numerous hospital visits. This solution has the potential to not only provide a strong wire alternative for toe fusion surgery but also an improved patient experience.

This study aimed to provide a proof of concept for the creation of an implantable SF-Mg composite capable of holding the joints of the toe in place for toe fusion surgery. Inherent strong thermoformable properties of the 1% SF thermoplastics allow for toe fusion in addition to incorporation of the native toe orientation shape, allowing for fusion and a more comfortable patient experience and subsequent outcomes.

Previously established design goals were achieved throughout this study. Specifically, a method of creating these thermoplastics was established in addition to making the cohesive composites themselves. In the future, improved machining practices such as more precise turning would allow for more consistent and uniform samples, preventing exposure of the Mg wire in the composite. In addition, creating a new molding system that does not require the use of a lathe would be advantageous to prevent any inconsistencies seen with machining.

Successful coating of the hydrophobic polymers on the Mg wires was accomplished and confirmed via AFM. In the future, alterations to the coating methodology for PLGA should be explored given the inconsistent coating. More specifically, a higher molecular weight PLGA, thicker coating, as well as less aggressive surface preparation should be explored. The dip coating of Cutin should be adjusted to heat it to its melting temperature, preventing any color change in the polymer. In addition, the process of combining HHA powder with 1% SF powder through an even distribution method should be further investigated. Simultaneously pressing the HHA and 1% SF powder in a thermopress not only could polymerize HHA into PHHA but also may produce a thermoformable thermoplastic. Developing a standardized method for this process and mechanically characterizing the resulting composite should also be explored.

The mechanical behavior of the 1% SF wires were found to be consistent with the behavior in previous literature and the reinforced composites, for the most part, were found to withstand higher mechanical stress[22]. The hydrated behavior of the wires should be further explored using improved three-point bending fixtures complete with a circular indent, which prevents movement during testing. Substituting the 99.9% Mg wire in the composites with commercial Mg alloys, as they become available in the future, is anticipated to enhance its strength, thereby optimizing the replacement for K-wires[30]. In addition, oscillatory three-point bending should also be conducted in the future to mimic physiological loading conditions for a more comprehensive understanding of the mechanical behavior.

The initial hypothesis indicated that the coated samples were expected to exhibit similar behavior as the 1% SF samples since the protease breaks down the silk proteins. However, since the coated samples contained the magnesium wire, this disrupted the overall structure of the composite, allowing for easier infiltration of the protease and subsequent faster degradation. As such, identifying methods to create better and more stable interactions between the coated Mg and the wire would allow for a more cohesive composite. Improved machining practices which prevent exposure of the embedded Mg wire would also aid in delaying degradation. Samples were capable of withstanding 30 days in protease solution while losing only about half of their mass, indicating their capability to hold the joints in place allowing for fusion which takes about 2-3 months based on the patient. Moving forward, a longer degradation study should be performed as it would provide more insight into the composite's behavior over a period of 2-3 months. Given the presented data, the SF-Mg composite wires have the potential to be a successful replacement for existing solutions use in toe joint arthrodesis.

References

1. Kramer WC, Parman M, Marks RM. Hammertoe correction with k-wire fixation. *Foot Ankle Int*. 2015;36(5):494-502. doi:10.1177/1071100714568013

2. Rajan L, Kim J, An T, et al. The influence of concomitant hammertoe correction on postoperative outcomes in patients undergoing hallux valgus correction. *Foot Ankle Surg Off J Eur Soc Foot Ankle Surg*. 2022;28(7):1100-1105. doi:10.1016/j.fas.2022.03.008

3. Camasta CA, Cass AD. BURIED KIRSCHNER-WIRE FIXATION FOR HAMMERTOE ARTHRODESIS.

4. Hammer Toes. Southernmost Foot & Ankle Specialists. Accessed June 28, 2024. https://urgentfootcare.com/conditions/hammer-toes/

5. Smith RW, Joanis TL, Maxwell PD. Great Toe Metatarsophalangeal Joint Arthrodesis: A User-Friendly Technique. *Foot Ankle*. 1992;13(7):367-377. doi:10.1177/107110079201300701

6. Ignacio AU. Postoperative Management of K-Wires in Percutaneous Foot Surgery. *Int J Foot Ankle*. 2021;5(2):054. doi:10.23937/2643-3885/1710054

7. Reece AT, Stone MH, Young AB. Toe fusion using Kirschner wire. A study of the postoperative infection rate and related problems. *J R Coll Surg Edinb*. 1987;32(3):158-159.

8. Smart Toe II. Accessed December 1, 2023. https://www.stryker.com/us/en/foot-and-ankle/products/smart-toe-ii.html

9. Biber R, Pauser J, Geßlein M, Bail HJ. Magnesium-Based Absorbable Metal Screws for Intra-Articular Fracture Fixation. *Case Rep Orthop*. 2016;2016:9673174. doi:10.1155/2016/9673174

10. Haslhofer DJ, Gotterbarm T, Klasan A. High Complication Rate and High Percentage of Regressing Radiolucency in Magnesium Screw Fixation in 18 Consecutive Patients. *J Pers Med*. 2023;13(2):357. doi:10.3390/jpm13020357

11. Krebs T. *Magnesium-Based, Bioresorbable Implants for Pediatric Elbow Fractures, a Single Center Pilot Study for Osteosynthesis With Magnezix Screws in Fractures of the Epicondylus Ulnaris and Condylus Radialis.* clinicaltrials.gov; 2023. Accessed December 31, 2022. https://clinicaltrials.gov/study/NCT04571905

12. Seitz JM, Lucas A, Kirschner M. Magnesium-Based Compression Screws: A Novelty in the Clinical Use of Implants. *JOM*. 2016;68(4):1177-1182. doi:10.1007/s11837-015-1773-1

13. Lee KY, Mooney DJ. Alginate: properties and biomedical applications. *Prog Polym Sci*. 2012;37(1):106-126. doi:10.1016/j.progpolymsci.2011.06.003

14. Gentile P, Chiono V, Carmagnola I, Hatton P. An Overview of Poly(lactic-co-glycolic) Acid (PLGA)-Based Biomaterials for Bone Tissue Engineering. *Int J Mol Sci*. 2014;15(3):3640-3659. doi:10.3390/ijms15033640

15. Rocher DH. WHITE PAPER - CONCLUSIONS STUDY FOR ABSORBABLE ACTIVAPIN™.

16. Song Y, Xu L, Jin X, Chen D, Jin X, Xu G. Effect of calcium and magnesium on inflammatory cytokines in accidentally multiple fracture adults. *Medicine (Baltimore)*. 2022;101(1):e28538. doi:10.1097/MD.0000000000028538

17. Cheng Y, Koh LD, Li D, Ji B, Han MY, Zhang YW. On the strength of β-sheet crystallites of *Bombyx mori* silk fibroin. *J R Soc Interface*. 2014;11(96):20140305. doi:10.1098/rsif.2014.0305

18. Nguyen PQ, Courchesne NMD, Duraj-Thatte A, Praveschotinunt P, Joshi NS. Engineered Living Materials: Prospects and Challenges for Using Biological Systems to Direct the Assembly of Smart Materials. *Adv Mater Deerfield Beach Fla*. 2018;30(19):e1704847. doi:10.1002/adma.201704847

19. Vepari C, Kaplan DL. Silk as a Biomaterial. *Prog Polym Sci*. 2007;32(8-9):991-1007. doi:10.1016/j.progpolymsci.2007.05.013

20. Holland C, Numata K, Rnjak-Kovacina J, Seib FP. The Biomedical Use of Silk: Past, Present, Future. *Adv Healthc Mater*. 2019;8(1):1800465. doi:10.1002/adhm.201800465

21. Polo-Corrales L, Latorre-Esteves M, Ramirez-Vick JE. Scaffold Design for Bone Regeneration. *J Nanosci Nanotechnol*. 2014;14(1):15-56. Accessed August 4, 2023. https://www.ncbi.nlm.nih.gov/pmc/articles/PMC3997175/

22. Guo C, Li C, Vu HV, et al. Thermoplastic Molding of Regenerated Silk. *Nat Mater*. 2020;19(1):102-108. doi:10.1038/s41563-019-0560-8

23. Rapid prototyping technology for bone regeneration. In: *Rapid Prototyping of Biomaterials*. Woodhead Publishing; 2014:289-314. doi:10.1016/B978-0-08-102663-2.00012-5

24. Thermoforming of high performance thermoplastic composites - Muzzy - 1990 - Polymer Composites - Wiley Online Library. Accessed July 29, 2024. https://4spepublications.onlinelibrary.wiley.com/doi/abs/10.1002/pc.750110505

25. Waizy H, Diekmann J, Weizbauer A, et al. In vivo study of a biodegradable orthopedic screw (MgYREZr-alloy) in a rabbit model for up to 12 months. *J Biomater Appl*. 2014;28(5):667-675. doi:10.1177/0885328212472215

26. Nidadavolu EPS, Feyerabend F, Ebel T, Willumeit-Römer R, Dahms M. On the Determination of Magnesium Degradation Rates under Physiological Conditions. *Materials*. 2016;9(8):627. doi:10.3390/ma9080627

27. Zhu Y, Liu W, Ngai T. Polymer coatings on magnesium-based implants for orthopedic applications. *J Polym Sci*. 2022;60(1):32-51. doi:10.1002/pol.20210578

28. Kligman A, Dastmalchi K, Smith S, John G, Stark RE. Building Blocks of the Protective Suberin Plant Polymer Self-Assemble into Lamellar Structures with

Antibacterial Potential. *ACS Omega*. 2022;7(5):3978-3989. doi:10.1021/acsomega.1c04709

29. Morgan EF, Unnikrisnan GU, Hussein AI. Bone Mechanical Properties in Healthy and Diseased States. *Annu Rev Biomed Eng*. 2018;20:119-143. doi:10.1146/annurev-bioeng-062117-121139

30. Wang P, Hamila N, Boisse P. Thermoforming simulation of multilayer composites with continuous fibres and thermoplastic matrix. *Compos Part B Eng*. 2013;52:127-136. doi:10.1016/j.compositesb.2013.03.045

31. Luo Y, Chen L, Shih A. Hollow Notched K-Wires for Bone Drilling With Through-Tool Cooling. *J Orthop Res*. 2019;37. doi:10.1002/jor.24419

32. Singha S, Gowda V, Hedenqvist MS. Plant Cuticle-Inspired Polyesters as Promising Green and Sustainable Polymer Materials. *ACS Appl Polym Mater*. 2021;3(8):4088-4100. doi:10.1021/acsapm.1c00585

33. Rockwood DN, Preda RC, Yücel T, Wang X, Lovett ML, Kaplan DL. Materials fabrication from Bombyx mori silk fibroin. *Nat Protoc*. 2011;6(10):1612-1631. doi:10.1038/nprot.2011.379

34. Gao L, Jia J, Kong X. A SNP-Based Molecular Barcode for Characterization of Common Wheat. *PLoS ONE*. 2016;11(3):e0150947. doi:10.1371/journal.pone.0150947

35. Li JN, Cao P, Zhang XN, Zhang SX, He YH. In vitro degradation and cell attachment of a PLGA coated biodegradable Mg–6Zn based alloy. *J Mater Sci*. 2010;45(22):6038-6045. doi:10.1007/s10853-010-4688-9

36. Mudgil D, Barak S. Chapter 2 - Classification, Technological Properties, and Sustainable Sources. In: Galanakis CM, ed. *Dietary Fiber: Properties, Recovery, and Applications*. Academic Press; 2019:27-58. doi:10.1016/B978-0-12-816495-2.00002-2

37. Sheng Y, Tian L, Wu C, Qin L, Ngai T. Biodegradable Poly(l-lactic acid) (PLLA) Coatings Fabricated from Nonsolvent Induced Phase Separation for Improving Corrosion Resistance of Magnesium Rods in Biological Fluids. *Langmuir ACS J Surf Colloids*. 2018;34(36):10684-10693. doi:10.1021/acs.langmuir.8b02322

38. Erdmann N, Angrisani N, Reifenrath J, et al. Biomechanical testing and degradation analysis of MgCa0.8 alloy screws: A comparative in vivo study in rabbits. *Acta Biomater*. 2011;7(3):1421-1428. doi:10.1016/j.actbio.2010.10.031

39. Francis LF. *Materials Processing: A Unified Approach to Processing of Metals, Ceramics and Polymers*. Elsevier; 2016.

40. Balogová AF, Trebuňová M, Bačenková D, et al. Impact of In Vitro Degradation on the Properties of Samples Produced by Additive Production from PLA/PHB-Based Material and Ceramics. *Polymers*. 2022;14(24):5441. doi:10.3390/polym14245441

41. Temenoff JS, Mikos AG. *Biomaterials: The Intersection of Biology and Materials Science*. Pearson/Prentice Hall; 2008.

42. Tsai SW. *Composite Materials: Testing and Design (Fifth Conference)*. American Society for Testing & Materials; 1979.

43. Kundu J, Pati F, Shim JH, Cho DW. Rapid prototyping technology for bone regeneration. In: *Rapid Prototyping of Biomaterials*. Elsevier; 2014:289-314. doi:10.1016/B978-0-08-102663-2.00012-5

44. STAINLESS STEEL 304L WIRE SOLUTIONS. Accessed July 25, 2024. https://www.scottprecisionwire.com/technical-data/alloy-data-sheets/stainless-steel-304l-wire/

45. Jayasathyakawin S, Ravichandran M, Baskar N, Anand Chairman C, Balasundaram R. Mechanical properties and applications of Magnesium alloy – Review. *Mater Today Proc*. 2020;27:909-913. doi:10.1016/j.matpr.2020.01.255

46. Jing X, Ding Q, Wu Q, et al. Magnesium-based materials in orthopaedics: material properties and animal models. *Biomater Transl*. 2021;2(3):197-213. doi:10.12336/biomatertransl.2021.03.004